Effect of Mn doping on structure, the dielectric and electric properties of BCZT ceramics

Ismail Khmiri[1] · Issa Kriaa[1] · Hamadi Khemakhem[1]

Abstract

The synthesis of $(Ba_{0.99}Ca_{0.01})(Zr_{0.2}Ti_{0.8})O_3$ (BCZT) and doped $(Ba_{0.99}Ca_{0.01})(Zr_{0.2}Ti_{0.8-x}Mn_x)O_3$ (BCZT-xMn) ceramics was successfully carried out by the solid-state method. The doping effect is followed by X-ray powder diffraction, scanning electron microscopy (SEM), and dielectric and conductivity measurements. Indeed, X-ray diffraction measurements show the crystalline structure of ceramics. SEM images indicate the doping effect on the studied perovskite microstructure. The results indicate that during doping the maximum value of the temperature (Tm) of the dielectric constant varies slightly, and there will be a considerable decrease in permittivity, dielectric losses and conductivity. Manganese ions are well integrated in the perovskite while maintaining the solid solution.

Keywords Dielectric · Ceramic · Ferroelectric · Permittivity

1 Introduction

Since the 1950s, the Pb-based ceramic perovskite compositions like $Pb(Zr_{1-x}Ti_x)O_3$ (PZT) and $PbMg_{1/3}Nb_{2/3}O_3$ (PMN) have been frequently used worldwide for their dielectric properties [1, 2]. This material has a very high dielectric permittivity at the Curie temperature and a coupling coefficient too. For this reason, it is found useful in various fields of applications such as transducers and sensors [3–5]. However, these lead oxides have recently been found to be toxic and seriously dangerous to the environment and human health. Much research has therefore been conducted to find its lead-free alternative with similar ferroelectric and piezoelectric effects, generally titanium-based solid solutions such as $Bi_{0.5}Na_{0.5}TiO_3$(NBT), $K_{0.5}Na_{0.5}NbO_3$ (KNN), $BaTiO3$ (BT) and $(Ba,Ca)(Ti,Zr)O_3$ (BCTZ) [6]. Among piezoelectric materials, we can mention the most famous one, (1-x) $Ba(Zr_{0.2}Ti_{0.8})O_3$-x$(Ba_{0.7}Ca_{0.3})TiO_3$ (BZT-xBCT), a pseudobinary system that had a very high piezoelectric coefficient of about 600pc/N at room temperature, an amazing value that even exceeds that of the PZT perovskites [7–10].

✉ Ismail Khmiri
   khmiriismail505@yahoo.fr

1   Laboratory of Multifunctional Materials and Applications (LaMMA), LR16ES18, Faculty of Sciences of Sfax, University of Sfax, Soukra road BP 1171, 3000 Sfax, Tunisia

Among the important characteristics of this pseudo-binary ferroelectric BCZT is the existence of a triple point in the previously studied BZT-BCT diagram, located at $x = 0.32$ where this region is considered as a separation between the rhombohedral and the tetragonal symmetry and corresponds to a high permittivity and huge electromechanical coefficients [11].

In fact, at the end of the last century, Simon et al. focused their researches on the ternary form $BaTiO_3$-$CaTiO_3$-$BaZrO_3$, which led to a diagram of four zones with different structures and dielectric aspects [2, 12], as shown in Fig. 1:

Zone 1: Dielectric behavior similar to $BaTiO_3$ in both its proximity and the $Ba_{1-x}Ca_xTiO_3$ (BT-CT), with three anomalies corresponding to rhombohedral (R), tetragonal (T), orthorhombic (O) and cubic (C) transitions.

R-O transition temperature decreases remarkably as the substitution of Ba^{2+} by Ca^{2+} increases in perovskite A sites.

Zone 2: For solid compositions close to $BaTi_{1-x}Zr_xO_3$ with $0.1 < x < 0.27$, only one dielectric anomaly is detected related to the R–C transition; the Curie temperature peak is remarkable without dispersion by frequency effect.

Zone 3: In $BaTi_{1-x}Zr_xO_3$ proximity with $0.275 < x < 0.42$, there is a larger peak with higher temperature values and a frequency dispersion. At the macroscopic scale, the compositions keep their shape and polarization regardless of the temperature.
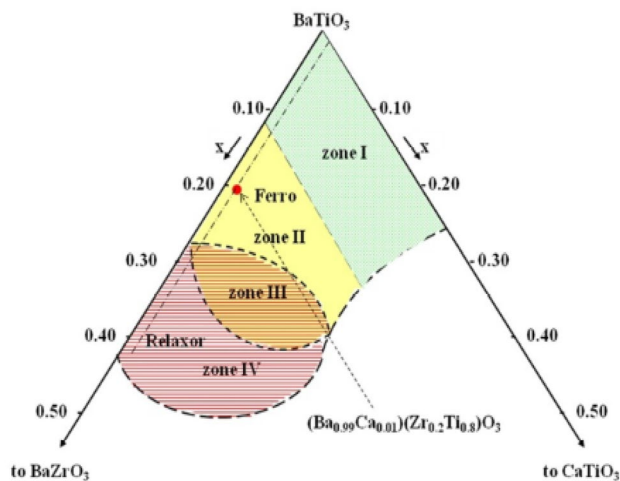
Fig. 1 Schematic representation of the BT–BZ–CT ternary diagram

Zone 4: This region separates zone II from zone III where, depending on the composition, classic ferroelectric states and relaxing states coexist.

However, the formation of the pure perovskite phase BCZT requires a very high calcinations and sintering temperature of about 1420 °C for sintering. The studies carried out by the researchers aim at reducing the temperature and improving the electrical presets of the perovskite.

The doping with various metal ions such as Ca^{2+} [13], Cu^{2+} [14], Fe^{3+} [14], Bi^{3+} [11], Mg^{2+} [14] and Mn^{4+} [15] either in site A or/and B can improve the properties of BCZT ceramics. As mentioned, the addition of a dopant to (BCZT) ceramics can improve densification, dielectric and ferroelectric properties. MnO_2 is an interesting additive because of its multivalence which can be a donor or acceptor dopant [16]. Research studies show that the addition of Mn can reduce dielectric losses and increase the densification of dielectric metals [5].

Mn doping at B sites of the perovskite $(Ba_{0.99}Ca_{0.01})$ $(Zr_{0.2}Ti_{0.8-x}Mn_x)O_3$ (BCZT-xMn) structure creates a variety of compositions with many properties similar to those of lead ceramics, such as cooling devices and dielectric responses enhanced by the rhombohedral (R) and tetragonal (T) phases separated by an intermediate orthorhombic (O) phase.

2 Experiment details

The lead-free BCZT-xMn ceramics were prepared by a solid state method where % $x =$ (0, 0.25 and 1). The starting materials with highly pure (99.9%) powders $BaCO_3$, $CaCO_3$, ZrO_2, TiO_2 and MnO_2 were dried in an oven heated to 150 °C for one hour. Then, they were then weighed to obtain a mixture with stoichiometric proportions.

The mixture was milled for 2 h, then pressed (100 MPa) into a cylindrical shape and followed by calcinations at 1150 °C for 15 h. The resulting pellet was grounded again into powder for 2 h to increase reactivity and reduce particle thickness to the micrometer. Subsequently, the powders obtained were reformed into pellets with a diameter of 8 mm and reheated at 1420 °C for 4 h.

The phase purity of the prepared ceramic was confirmed by X-ray powder diffraction (Philips X'Pert, Pro X-ray Diffractometer) using CuKα radiation ($\lambda = 1.5418$ A°). The evolution of grain size is observed by the SEM technique using a scanning electron microscope. A precision impedance analyzer shows the evolution of the dielectric permittivity in relation with the temperature.

3 Results and discussions

3.1 X-ray diffraction

Figure 2 depicts the X-ray diffraction of BCZT-xMn ceramics. Firstly, the diagram does not indicate the existence of other phases than the structured perovskite, which implies that the Mn^{4+} particles are well introduced into the unit cell of the perovskite in order to preserve the structure of the solid solution. The X-ray diagrams of the BCZT and BCZT-xMn ceramics reveal peak of diffraction at 45°, which is consistent with crystals (002) and (200), indicative of the tetragonal structure of BCZT ceramics.

In addition, the diffraction peaks are slightly shifted towards the widest angle for a higher Mn concentration indicating the decrease of the ceramic system constant (BCZT-Mn), which is linked in particular to the presence of Mn^{4+} occupying the B sites. In fact, the ionic radius of Mn^{4+}(0.54 A°) is smaller than that of Ti^{4+} (0.605 A°) and Zr^{4+} (0.72 A°).

On the other hand, the diffraction peaks of BCZT-xMn ceramics exhibit a full width at half maximum that increases with Mn concentration. This can be linked to the size of the ceramic grains (which decreases if the Mn content becomes higher).

The reticular planes of a crystal are defined by their Miller indices (hkl), or there is an interference of planes for the triplets (h,k,l) in orthorhombic structure. The interreticular distance d_{hkl} was related to the Miller indices by the following relationship [17, 18]:

$$\frac{1}{d_{hkl}^2} = \frac{h^2}{a^2} + \frac{k^2}{b^2} + \frac{l^2}{c^2} \tag{1}$$

with d_{hkl} is calculated from the Bragg equation [17–20]:
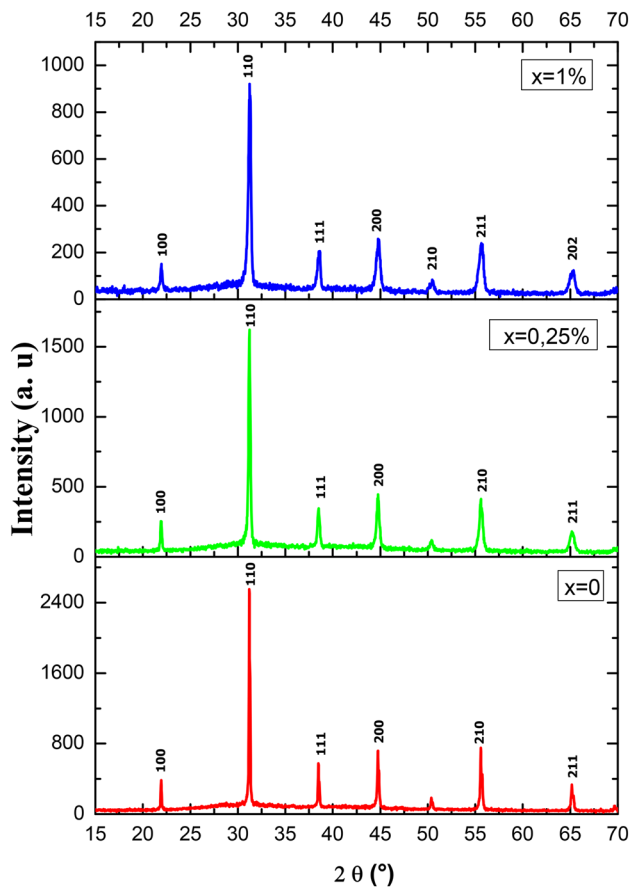
$$2d_{hkl} \sin\theta = n\lambda \tag{2}$$

Fig. 2 X-ray diffraction pattern of the Mn (0%, 0.25% and 1%) doped BCZT

Table 1 Lattice parameters of BCZT-xMn (% $x = 0$, 0.25 and 1)

BCZT-xMn	a (A)	b (A)	c (A)	c/a
x = 0%	4.0512	4.0447	4.0507	0.9998
x = 0.25%	4.0488	4.0474	4.0542	1.0013
x = 1%	4.0783	4.0033	4.0777	0.9998

where n is the order of diffraction taken equal to one in general ($n = 1$), and λ is the wavelength of X-ray diffraction equal to 1.5418A°.

The calculation of the lattice parameters a, b and c is shown in Table 1. These results indicate that the addition of Mn induces a slight variation in the lattice parameters. Indeed, the ionic radius of Mn^{4+} (0.54 A°) and Mn^{3+} (0.645 A°) is close to the ionic radius of Ti^{4+} (0.605A°). However, the radius of Mn^{2+} (0.83A°) is larger than that of Ti^{4+}, and the occupation of the Ti site by Mn ions induces a weak deformation of the crystal lattice.

The calculation of the nanometric dimensions of the BCZT-xMn ceramic particles is based on the study of ray diffraction; the size of the crystallites is given by the following Scherer's law [18, 21]:

$$D = \frac{K\lambda}{\beta \cos \theta} \tag{3}$$

where D is the size of the crystallites, λ is the wavelength of the X-rays (1.5418 A°), K is the Scherer constant taken equal to 0.9, θ is the diffraction peak angle, and β is the width at mid-height of the diffraction peaks (FWHM) determined by the Match refinement.

Thus, we can follow the epsilon micro-deformation according to the law [18]:

$$\varepsilon = \frac{\beta}{4 \cos \theta} \tag{4}$$

According to the figure illustrating the X-ray diffraction, the FWHM increases with the addition of Mn, which induces a remarkable decrease in the size of the nanocrystallites with the increase in the amount of dopant from 144.366 to 57.729 nm for the high intensity peak, corresponding to the Miller index (110) (Table2).

In fact, the diffusion of manganese ions into the ceramic leads to a reduction of the grain size which is mainly related to the appearance of oxygen vacancies. These results are grouped in Table 2.

Table 2 Grain size and microstrain of BCZT-xMn ceramics

	hkl	100	110	111	200	210	211	202
BCZT-xMn x = 0%	β	0.0998	–	–	0.1497	0.1996	0.1497	–
	D(nm)	141.63	144.366	147.272	100.242	76.831	104.776	110
	ε	0.1287	0.0892	0.0714	0.0090	0.0106	0.00710	0.0058
BCZT-xMn x = 0.25%	β	0.1497	0.2495	0.2994	0.2994	0.1996	0.3493	0.4491
	D (nm)	94.418	57.747	49.093	50.124	76.83	44.904	36.648
	ε	0.1929	0.2231	0.2142	0.1816	0.1060	0.1656	0.1759
BCZT-xMn x = 1%	β	0.2495	–	–	–	–	0.4990	0.5988
	D (nm)	56.637	57.729	58.878	60.072	61.452	31.407	27.483
	ε	0.3239	0.2240	0.1794	0.1527	0.1327	0.2376	0.2347

3.2 Surface morphology

Figure 3 displays the micrographs of the BCZT and BCZT-xMn ceramics using the SEM analysis. The images taken of the different samples clearly depict a non-homogeneous particle size distribution. The addition of a small amount of Mn in doped ceramics leads to a larger grain size than in BCZT ceramics. Such addition promotes the growth of the ceramic grains, and therefore, a substitution of the B-site with Mn^{3+} and Mn^{4+} ions will occur, leading to the creation of oxygen vacancies and an improved mass and energy transfer.

3.3 Dielectric study

To monitor the effect of Mn doping on the dielectric permittivity and dielectric losses of BCZT-xMn ceramics, measurements will be made for BCZT ceramics and both doped, and recorded in Fig. 2 for a frequency range from 1 to 1 MHz.

Figure 4 show that:

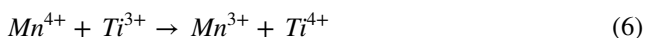(i) Maximum dielectric permittivity decreases with frequency.

(ii) For the BCZT ceramics (Fig. 4a), the maximum temperature is close to room temperature and there is a slight dispersion at maximum.

(iii) Both curves correspond to Mn-doped ceramics (Fig. 4b and c); the peak widens as soon as the amount of Mn increases and the dielectric maximum decreases with a temperature shift associated with the maximum permittivity. It is also noted that there is a slight dispersion of the permittivity for $T \leq T_m$ and the dielectric losses decrease with temperature for all samples.

Indeed, Ti^{4+} ions are less chemically stable and are reduced to Ti^{3+} ions according to Eq. (5):

$$Ti^{4+} + \frac{1}{2}O_o^x \rightarrow Ti^{3+} + \frac{1}{2}V_o^- \tag{5}$$
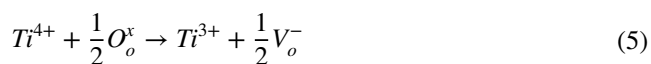
When the Mn^{4+} ions diffuse into the BCZT ceramic, they are substituted with the Ti^{3+} ions according to the reaction (6):

$$Mn^{4+} + Ti^{3+} \rightarrow Mn^{3+} + Ti^{4+} \tag{6}$$

This is notably linked to Mn additions, which limit the concentration of vacant oxygen positions and causes the decrease of the permittivity [22].

The dielectric permittivity in the paraelectric zone for a normal ferroelectric is given by the following Curie Weiss formula (7):

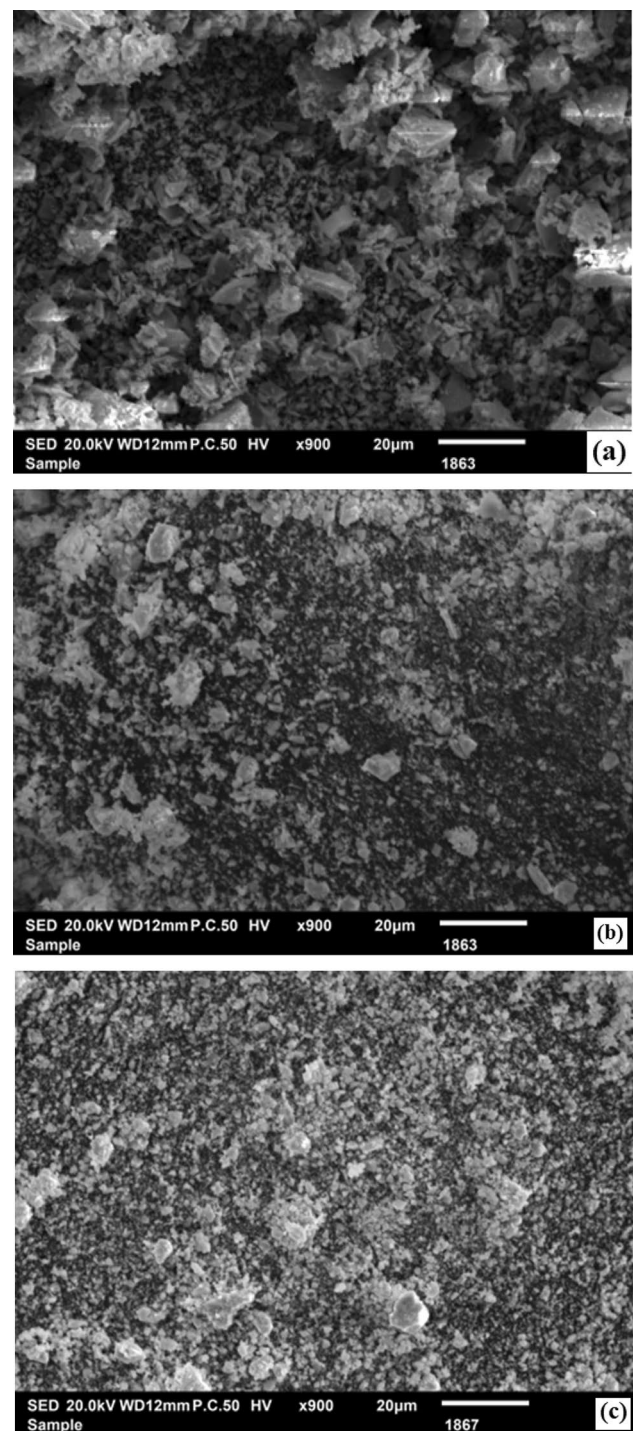$$\varepsilon_r'(T) = \frac{C}{T - Tm} \tag{7}$$

Fig. 3 SEM micrographs of surface BCZT-xMn ceramics (**a**: $x = 0\%$, **b**: 0.25% and **c**: 1%)

where C and T_0 are the Curie constant and Curie temperature, respectively. The deviation from the Curie law is due to the assembly of short-range nanopolar domains [23].

Uchino and Nomura proposed another form for the previous law of Curie–Weiss given by Eq. (8) [23, 24]:
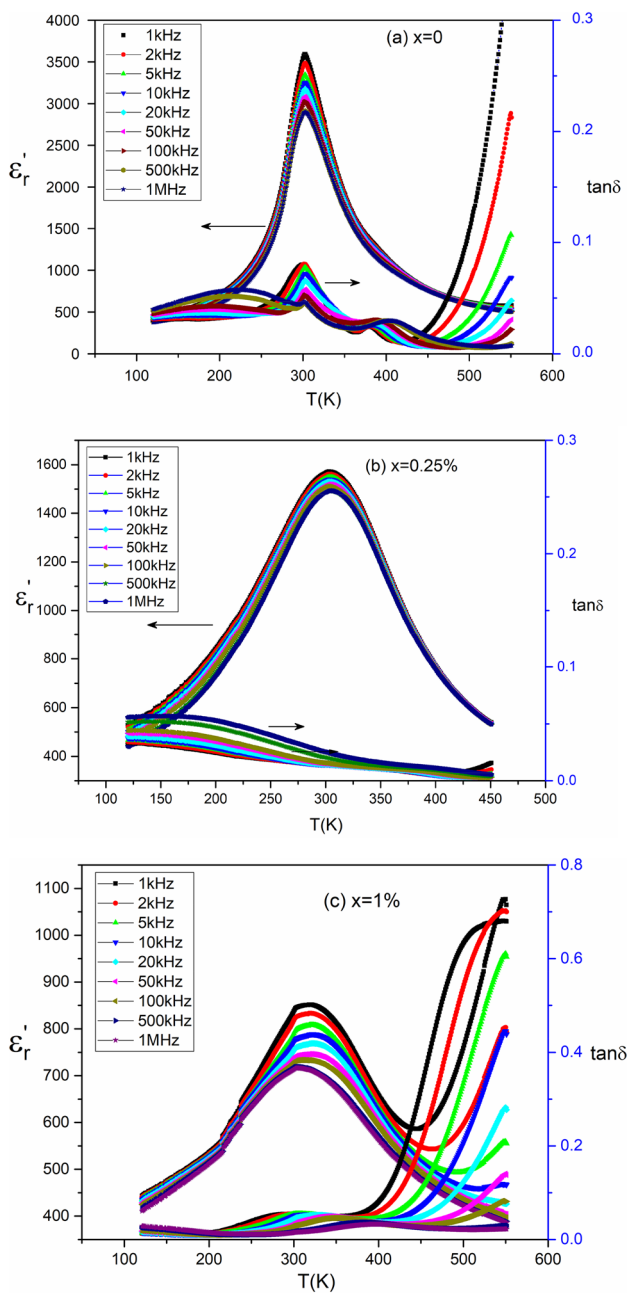
Fig. 4 Temperature dependence of dielectric constant and loss for BCZT-xMn ceramics

$$\frac{1}{\varepsilon'_r} - \frac{1}{\varepsilon'_{r\,max}} = \frac{(T - Tm)^{\gamma}}{C} \tag{8}$$

where $\varepsilon'_{r\,max}$ is the maximum permittivity of ceramics, and C is a multiplicative constant.

γ is a constant corresponding to the degree of diffuseness [22, 25, 26], and it gives information on the phase transition in perovskite determined by the linear fit of the experimental data.

A plot of $\ln\left(\frac{1}{\varepsilon'_r} - \frac{1}{\varepsilon'_{r\,max}}\right) = f\left(\ln T - T_m\right)$ drawn for $T>T_c$ for a frequency of 1 kHz allows us to obtain the value of γ (Table 3).

The relaxation behavior is described by the quantity ΔT_{relax} defined by:

$$\Delta T_{relax} = T_m(100\ kHz) - T_m(1\ kHz) \tag{9}$$

This relaxation parameter increases from 1 to 2 with the growth of the quantity of Mn added (Table 3).

Figure 5 illustrates the variations of permittivity as a function of temperature for $f = 1$ kHz; it allows us to go back to the values of maximum temperature T_m relative to the maximum of dielectric permittivity, critical temperature T_0 and temperature T_d from which the dielectric constant starts to deviate from Curie's law Figure 6. For this purpose, the degree of deviation from the Curie–Weiss law can be described by means of parameters ΔT_m defined as follows:

$$\Delta T_m = T_d - T_m \tag{10}$$

The values of this parameter increase if Mn concentration increases which suggests that Mn doping induces a diffusion of the ceramic phase transition BCZT, where the diffuseness character of the phase transition is described by the following empiric parameter:

$$\Delta T_{diff} = T_{0.9\varepsilon_{r\,max}}(1\ kHz) - T_{\varepsilon_{r\,max}}(1\ kHz) \tag{11}$$

The value of this parameter indicates the effect of doping ceramics BCZT-xMn. The main values extracted from the study on the ceramic dielectric of BCZT doped Mn are summarized in Table 3.

Figure 7 describes the variations of dielectric permittivity and dielectric losses as a function of frequency for $T = T_m$ for a range from 1 to 1000 kHz. In this range, the dielectric constant is reduced as the frequency increases
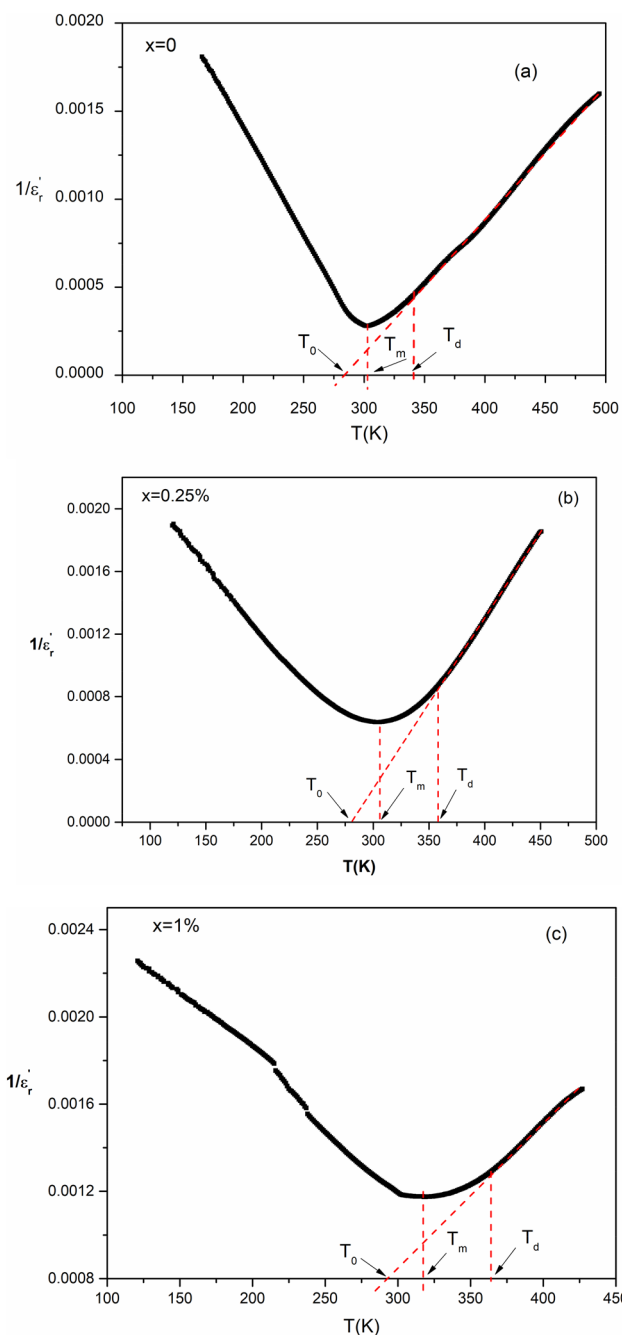
Table 3 Dielectric properties of BCZT-xMn ceramics	% x	T_m(K)	ε_m at 1 kHz	ΔT_{diff} (K)	ΔT_m(K)	ΔT_{relax}(K)	γ
	0	302	3570.91	11.75	33.89	1.045	1.29
	0.25	304	1570.32	28.3	57.65	1.568	1.89
	1	317	850.29	51.58	59.8	2.091	1.92

Fig. 5 Temperature dependence of inverse dielectric constant for BCZT-xMn ceramics

Fig. 6 $\ln(1/\varepsilon - 1/\varepsilon_{max})$ as a function of $\text{Ln}(T-T_m)$ for the BCTZ-xMn ($x = 0\%$, 0.25% and 1%) ceramics at 10 kHz

and decreases with Mn content due to the reduction in particle size with MnO_2 doping. The dielectric losses vary slightly with frequency, and a minimum value of around 0.01 can be recorded.

Figure 8 shows the conductivity measured at the critical temperature T_m as a function of the frequency of the BCZT ceramic. It is defined according to the following relationship:
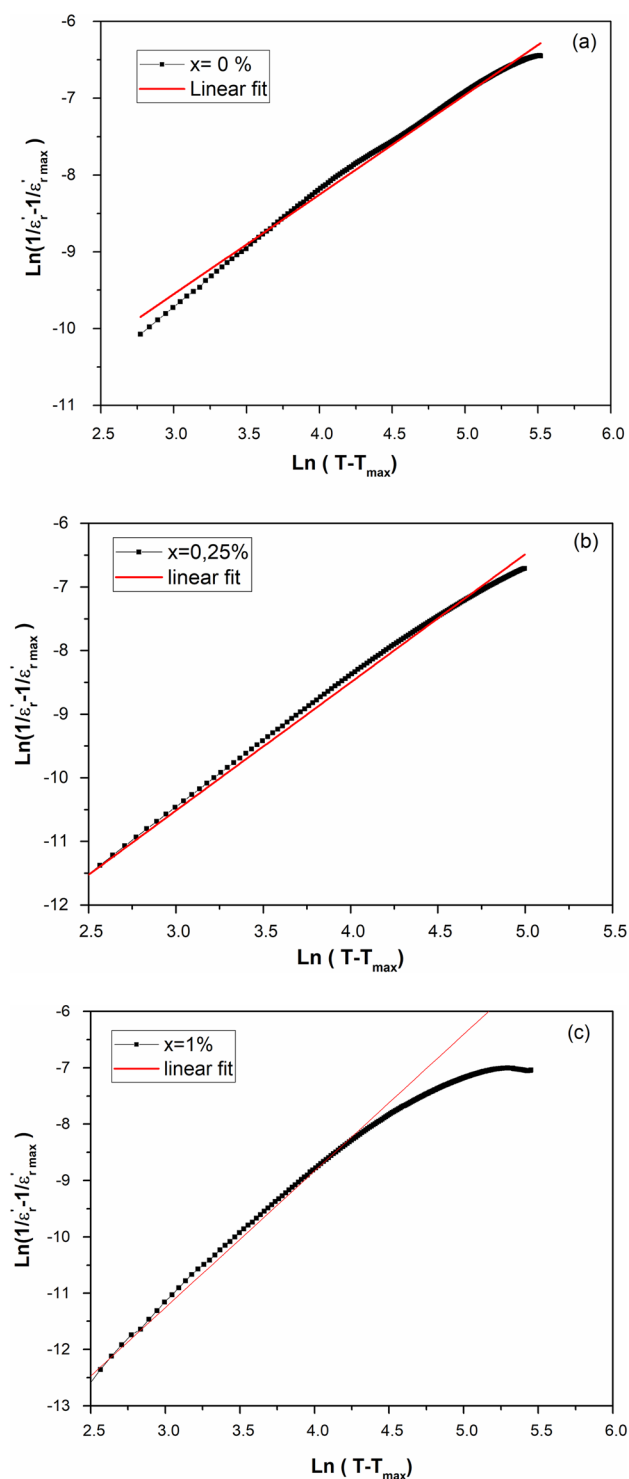
$$\sigma_{ac} = \omega \varepsilon_0 \varepsilon_1 \tan \varepsilon_1 \tag{12}$$

where ω is the angular frequency, both ε_0 and ε_1 are the dielectric constants of vacuum and the relative dielectric
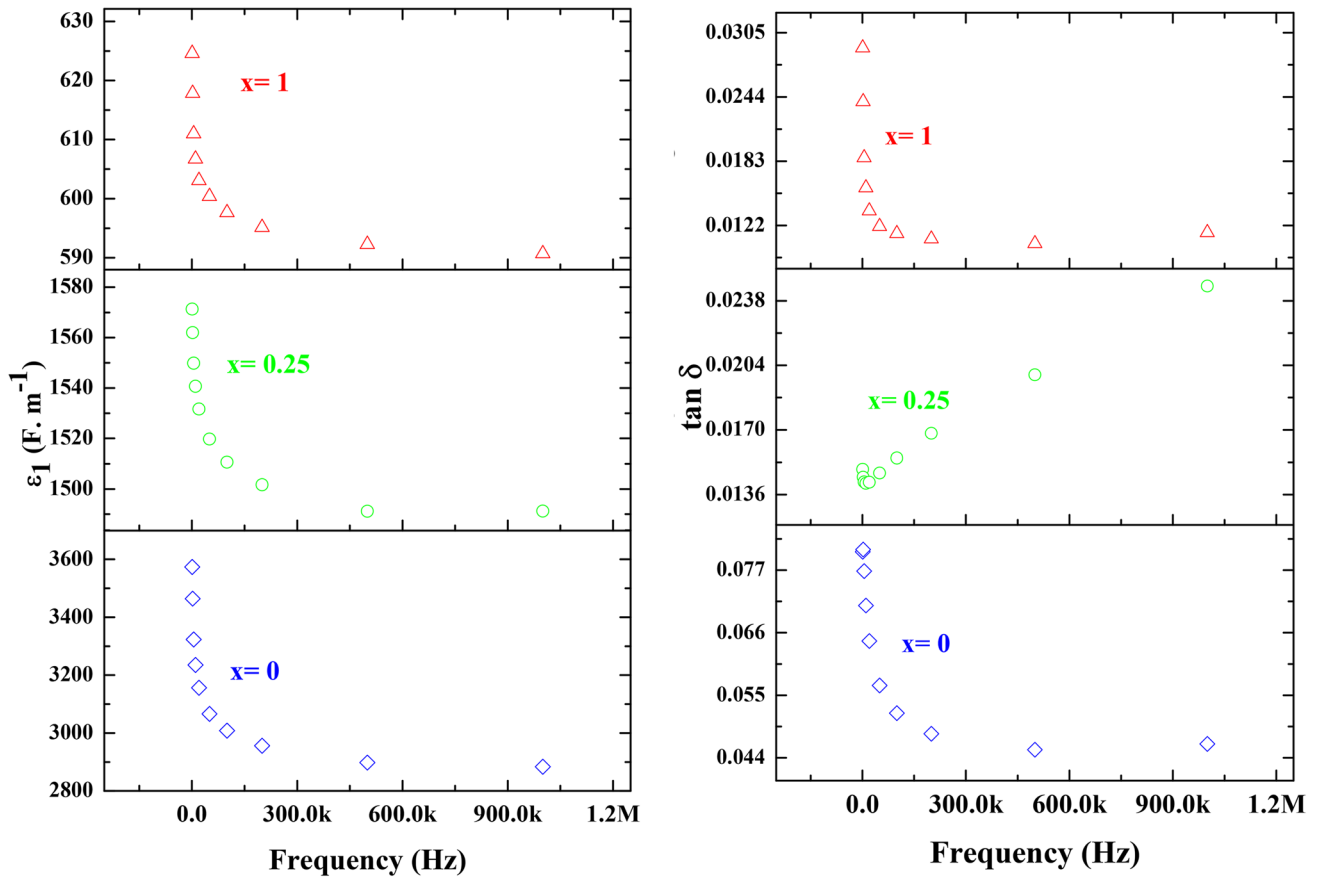
Fig. 7 Dielectric constant and dielectric loss as functions of frequency for BCZT-xMn ceramics at T = T$_m$
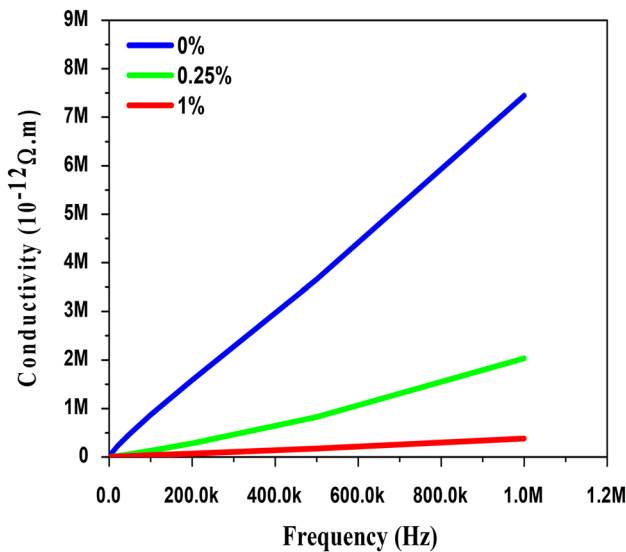

Fig. 8 AC conductivity as function of frequency for Mn doped for BCZT-xMn (%x = 0, 0.25 and 1) at T$_m$

constant, and $tan\varepsilon_1$ is the dielectric loss. However, it can be seen that conductivity is highly frequency dependent and

follows a linear variation. It increases with frequency, which implies a decrease in resistance according to the law:

$$R = \frac{l}{\sigma \, S} \tag{13}$$

The conductivity also reduces with Mn doping as a result of the presence of defects or impurities in the ceramic.

4 Conclusion

BCZT and BCZT-xMn-doped ceramics are successfully prepared by the solid–solid method. The DRX spectra highlight the presence of the pure phase of the material, indicating that the Mn^{4+} ions are well integrated in the perovskite while maintaining the solid solution.

The addition of Mn reduces the permittivity of doped ceramics and reduces dielectric losses. In fact, the addition of manganese oxide reduces the concentration of vacant oxygen by occupying the perovskite site B while substituting with Ti^{4+} ions and also reduces the size of the grains.

In fact, DRX shows that the Mn doping decreases the granular size, in accordance with the values of the crystallite size which evolves from 144.36 nm for the parent compound up to 57.729 nm for an addition of 1% of Mn for the main peak (110). The low deformation of the perovskite is given by constant epsilon called micro-deformation. The calculation of the mesh parameters indicates an orthorhombic structure of the ceramics.

SEM characterization allows us to trace the microstructure of ceramic compounds. The study of the dielectric part as a function of temperature for a frequency range from 1 kHz to 1 MHz indicates that the maximum relative permittivity (at temperature T_m for 1 kHz) decreases by adding Mn of 3570.91 for $x = 0\%$, 1570.32 for $x = 0.25\%$ to 850.29 for $x = 1\%$. The curve $\ln(1/\varepsilon - 1/\varepsilon_m) = f(\ln(T - T_m))$ allows us to know the nature of the phase transition by following the values of the diffusion coefficient which varies between 1 and 2. As well as the degree of deviation and the character of diffusion are, respectively, given by ΔT_{diff} and ΔT_d at the frequency 1 kHz. The decrease in permittivity and dielectric losses as a function of frequency at maximum temperature can also be marked for each composition.

A study of the conductivity shows that it varies linearly as a function of the frequency at temperature Tm for each proportion of Mn.

References

1. D.S. Keeble, F. Benabdallah, P.A. Thomas, M. Maglione, J. Kreisel, Revised structural phase diagram of (Ba0.7Ca0.3TiO3)-(BaZr0.2Ti0.8O3). Appl. Phys. Lett **102**, 092903 (2013)
2. A. Hamza, F. Benabdallah, I. Kallel, L. Seveyrat, L. Lebrun, H. Khemakhem, Effect of rare-earth substitution on the electrical properties and Raman spectroscopy of BCTZ ceramics. J. Alloy. Compd. **735**, 2523 (2018)
3. M. Siddiqui, J.J. Mohamed, Z.A. Ahmad, Structural, piezoelectric, and dielectric properties of PZT-based ceramics without excess lead oxide. J Aust Ceram Soc **56**, 371 (2020)
4. C. Xu, Z. Yao, K. Lu, H. Hao, Z. Yu, M. Cao, H. Liu, Enhanced piezoelectric properties and thermal stability in tetragonal-structured (Ba, Ca)(Zr, Ti)O piezoelectrics substituted with trace amount of Mn. Ceram. Int. **42**, 16109 (2016)
5. P. Parjansri, K. Pengpat, G. Rujijanagul, T. Tunkasiri, U.S. Intatha, Eittssayeam Effects of Mn and Sr Doping on the Electrical Properties of Lead-Free 0.92BCZT-0.08BZT. Ceram Ferroelectr **458**(1), 91–97 (2014)
6. D. Maurya, M. Peddigari, M.-G. Kang, L.D. Geng, N. Sharpes, V. Annapureddy, H. Palneedi, R. Sriramdas, Y. Yan, H.-C. Song, Y.U. Wang, J. Ryu, S. Priya, Lead-free piezoelectric materials and composites for high power density energy harvesting. J. Mater. Res. **33**, 2235 (2018)
7. W. Liu, X. Ren, Large piezoelectric effect in Pb-Free ceramics. Phys. Rev. Lett. **103**, 257602 (2009)
8. D. Damjanovic, A. Biancoli, L. Batooli, A. Vahabzadeh, J. Trodahl, Elastic, dielectric, and piezoelectric anomalies and Raman spectroscopy of 0.5Ba(Ti0.8Zr0.2)O3-0.5(Ba0.7Ca0.3)TiO3. Appl. Phys. Lett **100**, 192907 (2012)
9. A.T. Dang, T.T. Vo, V.C. Truong, V.H. Le, Influence of sintering temperature on structure, microstructure and piezoelectric properties of doped BZT{BCT ceramics. Int. J. Mod. Phys. B **31**, 1650258 (2016)
10. A.D. Loreto, A. Frattini, R. Machado, O. de Sanctis, M.G. Stachiotti, Preparation and characterization of Mn-doped (Ba0.85 ca0.15)(Zr0.1 Ti0.9)O3Ceramics. Ferroelectrics **463**, 105 (2014)
11. N. Othmani, A. Amouri, F. Benabdallah, Z. Sassi, L. Seveyrat, L. Lebrun, V. Perrin, H. Khemakhem, Effect of bismuth doping on structural and electrical properties of 0.9(BaZr0.2Ti0.8O3)–0.1(Ba0.7Ca0.3TiO3) ceramic. Ceram Int **46**, 22592 (2020)
12. J. Ravez, C. Broustera, A. Simon, Lead-free ferroelectric relaxor ceramics in the BaTiO-BaZrO3-CaTiO3system. J. Mater. Chem. **9**, 1609 (1999)
13. H. Kaddoussi, A. Lahmar, Y. Gagou, B. Manoun, J.N. Chotard, J.L. Dellis, Z. Kutnjak, H. Khemakhem, B. Elouadi, M. Elmarssi, Sequence of structural transitions and electrocaloric properties in ceramics. J Alloys Compd **713**, 164 (2017)
14. P. Jaiban, P. Wannasut, R. Yimnirun, A. Watcharapasorn, Influences of acceptor dopants (Cu Mg Fe) on electrical and optical properties of Ba0.7Ca0.3TiO3 ceramics. Mater Res Bullet **118**, 110501 (2019)
15. F. Feng, Y. Yan, Large electrostrictive effect in Mn-doped BCZT ferroelectric ceramics. Ceram. Int. **45**, 21315 (2019)
16. P. Parjansri, S. Eittssayeam, Effects of MnO2doping on the electrical properties BCZT ceramics prepared by seed-induced method. Ferroelectrics **534**, 63 (2018)
17. O. Kamoun, A. Boukhachem, M. Amlouk, S. Ammar, Physical study of Eu doped MoO3 thin films. J. Alloy. Compd. **687**, 595 (2016)
18. B. Gharbi, A. Boukhachem, M. Amlouk, M. Oueslati, B. Dkhil, A. Meftah, Physical investigations on LaMn1xNixO3perovskite sprayed thin films along with surface magnetic applications. Appl. Phys. A **126**, 604 (2020)
19. A. Loukil, A. Boukhachem, M. Ben Amor, M. Ghamnia, K. Raouadi, Effects of potassium incorporation on the structural, optical, vibrational and electrical properties of NiO sprayed thin films for p-type optical windows. Ceram Int **42**, 8274 (2016)
20. G. Bousselmi, N. Khemiri, A. Benali, M.P.F. Graca, R.F. Santos, B.F.O. Costa, M. Kanzari, Synthesis and study of structural, optical, and electrical properties of nontoxic and earth-abundant Na2ZnSnS-4material. J Mater Sci: Mater Electron **31**, 18858 (2020)
21. A. Boukhachem, M. Mokhtari, N. Benameur, A. Ziouche, M. Martínez, P. Petkova, M. Ghamnia, A. Cobo, M. Zergoug, M. Amlouk, Structural optical magnetic properties of Co doped α-MoO3sprayed thin films. Sens Actuat A Phys **253**, 198 (2017)
22. W. Cai, C. Fu, J. Gao, X. Deng, Effect of Mn doping on the dielectric properties of BaZr0.2Ti0.8O3ceramics. J Mater Sci: Mater Electron **21**, 317 (2010)
23. I. Djemel, I. Kriaa, N. Abdelmoula, H. Khemakhem, The effect of low Sn doping on the dielectric and electrocaloric properties of ferroelectric ceramics Ba0.95Sr0.05Ti0.95Zr0.05O3. J Alloys Compd **720**, 284 (2017)
24. K. Uchino, S. Nomura, Critical exponents of the dielectric constants diffused-phase-transition crystals. Ferroelectrics **44**, 55 (1982)
25. F. Bahri, H. Khemakhem, Relaxor behavior and dielectric properties of solid solution. J Alloys Compd **593**, 202 (2014)
26. L. Khemakhem, I. Kriaa, M. Derbel, N. Abdelmoula, X-ray and dielectric studies of ferroelectric phase in the Ba1-x(Yb0.5Na0.5)x TiO3 system for low doping level. Int. J. Nanoelectr Mater **2**, 137–145 (2009)